



# Prediction of multiple dominant chatter frequencies in milling processes

Zoltan Dombovari<sup>a,\*</sup>, Alex Iglesias<sup>b</sup>, Mikel Zatarain<sup>b</sup>, Tamas Insperger<sup>a</sup>

<sup>a</sup> Department of Applied Mechanics, Budapest University of Technology and Economics, Budapest H-1521, Hungary

<sup>b</sup> Dynamics and Control, Ideko-IK4, Elgoibar, Gipuzkoa 20870, Spain

## ARTICLE INFO

### Article history:

Received 28 October 2010

Received in revised form

4 February 2011

Accepted 7 February 2011

Available online 15 February 2011

### Keywords:

High speed machining

Regenerative effect

Delay differential equation

Self-excited frequencies

Semi-discretization

Chatter

## ABSTRACT

Chatter frequencies of milling operations and their strengths are analysed using the semi-discretization method. It is known that milling processes, being parametrically excited systems, are theoretically associated with infinitely many chatter frequencies that are given as a base frequency plus an integer multiplier of the tooth passing frequency (or the characteristic frequency of the cutter) according to the Floquet theory [1]. The dominant vibration frequencies that are usually associated with chatter frequencies are, however, hidden among the infinitely many harmonics. In this paper, it is shown that the amplitudes corresponding to the individual frequency harmonics can be determined in a simple way by analysing the eigenvectors of the Floquet transition matrix obtained by the semi-discretization method without increasing the computational cost. The method can be used to determine the dominant frequency components that help in the identification of the interactions between different modes and the spindle speed.

© 2011 Elsevier Ltd. All rights reserved.

## 1. Introduction

It is well known in the industry that besides the power and torque limits of the machine, the emerging self-excited vibration (the chatter) can also limit the machining productivity. Therefore, the stability predictions are more and more appreciated, especially for production lines, since the machines should be already calibrated roughly at the design stage. Apart from the limit depths of cut provided by the stability charts, the frequencies of the self-excited vibrations are of importance, too, since they can help to tune different parts of the machine to avoid chatter.

In practise, two major goals can arise at the design stage of a machine tool. On the one hand, the machine needs good static accuracy to reproduce the desired shape of the workpiece with good quality. This depends on the static stiffness and the control of the machine tool. On the other hand the machine has to handle the desired operation (e.g. roughing) without any instabilities, which requires good dynamical arrangement of the structure. At this stage, the prediction of the dominant frequencies and their possible strong harmonics is of importance since the weak modes of the machine can be identified and the structure can be tuned according to the calculated spectrum. Also, in machining diagnosis, it is important to know the possible sources of any

vibrations and separate them from the predicted chatter spectrum to realize e.g. bearing faults.

The theory of the regeneration in machining was derived by Tlustý [2] and Tobias [3] in the middle of the 20th century. They pointed out that the regeneration, especially in turning and in milling, can cause instabilities. They also showed that stable pockets exist in the high speed region, allowing the usage of extremely high depths of cut, which can lead to high productivity. These stability regions highly depend on the modal behaviour of the machines. Some machining operations like aluminium machining usually work with high-frequency modes related to the tool-toolholder, while some other materials, such as difficult-to-cut materials [4], operate the low-frequency structural modes. Consequently, the machine has to be dynamically designed to fit the required cutting operation.

In the literature one can find several numerical techniques developed to predict the linear stability of milling processes. There are methods based on frequency domain, such as the single-frequency (SF) [5] and the multiple-frequency (MF) [6,7] solutions, while the semi-discretization (SD) [8] and the time-finite element [9] are methods based on time domain. For completeness, there are continuation software packages for general anholonome delay-differential equations (DDE), e.g. PDDE-CONT [10], which are capable to perform both linear and nonlinear analysis of certain delayed systems. Generally, the methods based on frequency domain can provide the dominant vibration frequency, but they cannot handle general milling processes (e.g. serrated cutters [11–13]) and the rigorous linearization of nonlinear milling models.

\* Corresponding author.

E-mail addresses: [dombo@mm.bme.hu](mailto:dombo@mm.bme.hu), [ddombo@gmail.com](mailto:ddombo@gmail.com) (Z. Dombovari), [aiglesias@ideko.es](mailto:aiglesias@ideko.es) (A. Iglesias), [mzatarain@ideko.es](mailto:mzatarain@ideko.es) (M. Zatarain), [inspi@mm.bme.hu](mailto:inspi@mm.bme.hu) (T. Insperger).

As opposed to turning processes, milling operations are theoretically associated with infinitely many self-excited frequencies (chatter frequencies) according to the Floquet theory of DDEs [14] as it was shown in [1]. However, the identification of the dominant frequencies is not trivial. The frequency domain methods, the SF and the MF solutions, can provide the strengths of the harmonics, although these methods were mostly used to plot the dominant frequencies only. In this paper it is shown that the SD method is also able to derive the strengths of the multiple chatter frequencies in an efficient way. Moreover, the presented method can give the spectra of the just developing self-excited vibration for more complex milling models implemented in time domain.

In the first part of the paper we show the connection between the Floquet theory and the dominant vibration frequency using rigorous mathematical derivation. The method is based on the general representation of milling processes and it has no significant effect on the computation time of the SD method. In the second part of the paper we present a case study using the example from [15]. Through this example one can realize how the self-excited frequencies can interact with other modes in the system. A simple but useful frequency plot is introduced here to understand the relationship between the self-excited frequencies and the dynamics of the machine. In the last section, the theoretical results are verified by experimental tests.

### 2. Milling model

The relative vibration of the tool-tip is described in modal space defined by the modal coordinates  $\mathbf{q} = \text{col}(q_1, q_2, \dots, q_n)$  (see Fig. 1). The modes are supposed to be real, that is, the damping is proportional, consequently, the equations of motion have the following form

$$\ddot{\mathbf{q}}(t) + [2\xi_l \omega_{n,l}] \dot{\mathbf{q}}(t) + [\omega_{n,l}^2] \mathbf{q}(t) = \mathbf{U}^T \mathbf{F}(t, \mathbf{q}(t), \mathbf{q}(t-\tau_j)), \quad j = 1, \dots, N_\tau, \tag{1}$$

where  $[2\xi_l \omega_{n,l}]$  and  $[\omega_{n,l}^2]$  are  $(n \times n)$  diagonal matrices with  $\xi_l$  and  $\omega_{n,l}$  being the damping ratio and the natural angular frequency of the  $l$ th mode ( $l = 1, \dots, n$ ). Due to the regenerative effect, the resultant cutting force  $\mathbf{F}$  depends on the current modal coordinate vector  $\mathbf{q}(t)$  and  $N_\tau$  previous ones  $\mathbf{q}(t-\tau_j)$ , where  $N_\tau$  is the number of regenerative delays occurring in the system. Note that  $\mathbf{F}$  already contains the cutting force contributions of all flutes.

This general representation of the milling operation describes multiple delay cases that typically occur for non-uniform pitch angle tool [16] or for serrated tools [11,13] in contrast with the conventional models with a single delay being equal to the tooth passing period. In (1), the force is distributed to the modal

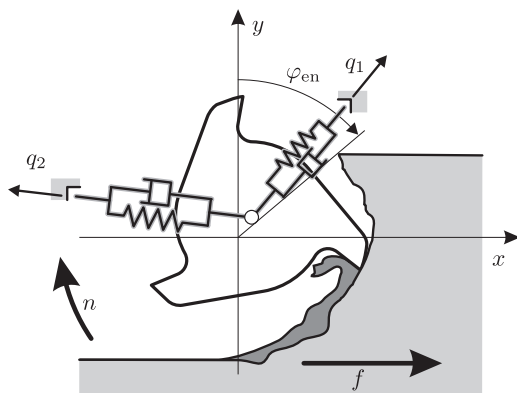


Fig. 1. Schematic model of milling process with general modes.

directions by the mass normalized modal matrix

$$\mathbf{U} = \mathbf{P} \text{diag}(c_l), \quad \text{where} \quad \mathbf{P} = [\mathbf{P}_1 \mathbf{P}_2 \dots \mathbf{P}_n],$$

$\mathbf{P}_l$  is the modeshape vector and  $c_l = (\mathbf{P}_l^T \mathbf{P}_l m_l)^{-1/2}$  is the normalization parameter of the  $l$ th mode, where  $m_l$  is the modal mass corresponding to  $\mathbf{P}_l$ . Since, the tool is rotating, (1) is time-periodic at period  $T$ , which is the tooth passing period or an integer divisor of the rotation period depending on the type of the cutter. The solution can be rewritten as the sum of a stationary and the perturbed motion, thus

$$\mathbf{q}(t) = \mathbf{q}_p(t) + \mathbf{u}(t), \quad \mathbf{q}_p(t) = \mathbf{q}_p(t+T). \tag{2}$$

The linear variational system of (1) can be determined in the form

$$\ddot{\mathbf{u}}(t) + [2\xi_l \omega_{n,l}] \dot{\mathbf{u}}(t) + ([\omega_{n,l}^2] + \mathbf{H}(t)) \mathbf{u}(t) = \sum_{j=1}^{N_\tau} \mathbf{H}_j(t) \mathbf{u}(t-\tau_j),$$

where the coefficient matrices are

$$\mathbf{H}_j(t) = \frac{\partial \mathbf{F}}{\partial \mathbf{q}(t-\tau_j)}(t, \mathbf{q}_p(t), \mathbf{q}_p(t-\tau_j)), \quad \mathbf{H}(t) = \sum_{j=1}^{N_\tau} \mathbf{H}_j(t). \tag{3}$$

Note that these matrices are also time-periodic at  $T$ , that is,  $\mathbf{H}_j(t) = \mathbf{H}_j(t+T)$ . Consider that, if (1) is linear, then  $\mathbf{H}_j(t)$  is equal to the coefficient of  $\mathbf{q}(t-\tau_j)$  in  $\mathbf{F}$  and the costly calculation of  $\mathbf{q}_p$  by the boundary value problem defined by (2) and (1) is not necessary. Finally, the dynamic model can be prepared for linear stability analysis in its first order representation [17] as

$$\dot{\mathbf{y}}(t) = \mathbf{L}(t) \mathbf{y}(t) + \sum_{j=1}^{N_\tau} \mathbf{R}_j(t) \mathbf{y}(t-\tau_j), \tag{4}$$

where  $\mathbf{L}(t) = \mathbf{L}(t+T)$  and  $\mathbf{R}_j(t) = \mathbf{R}_j(t+T)$ 's are the linear and the retarded time-periodic matrices and the new coordinates are defined as

$$\mathbf{y}(t) = \begin{bmatrix} \mathbf{u}(t) \\ \dot{\mathbf{u}}(t) \end{bmatrix}. \tag{5}$$

The stability of (4) can now be analysed using the SD method.

### 3. Stability of the variational system

According to the theory of DDEs [18,19], the linearized equations of motion at (4) generates an infinite dimensional function space defined by the shift as

$$\mathbf{y}_t(\theta) = \mathbf{y}(t+\theta),$$

where  $\theta \in [-\tau_{\max}, 0]$  and  $\tau_{\max} = \max(\tau_1, \tau_2, \dots, \tau_{N_\tau})$ . Using an arbitrary initial state  $\mathbf{y}_0(\theta)$  the solution can be given by the so-called fundamental operator  $U(t)$  in the following way

$$\mathbf{y}_t(\theta) = (U(t) \mathbf{y}_0)(\theta),$$

where the linear operator  $U(t)$  gives the connection between the actual state  $\mathbf{y}_t(\theta)$  and the initial state  $\mathbf{y}_0(\theta)$ . According to the extension of the Floquet theorem to DDEs [14], the stability of the system is fully determined by the fundamental operator which maps the initial state  $\mathbf{y}_0(\theta)$  to  $\mathbf{y}_T(\theta)$ , the corresponding monodromy operator is  $U(T)$ . The solution after one period is given by

$$\mathbf{y}_T(\theta) = (U(T) \mathbf{y}_0)(\theta). \tag{6}$$

Moreover, the Floquet theorem also claims that a general solution at the present time can be written as a product of a time-periodic and an exponential term in the form

$$\mathbf{y}_t(0) = \mathbf{y}(t) = \mathbf{a}(t) e^{\lambda t}, \tag{7}$$

where  $\mathbf{a}(t) = \mathbf{a}(t+T)$  and the complex number  $\lambda$  is called characteristic exponent. In this manner, an element of the function space at the period  $T$  is given by

$$\mathbf{y}_T(\theta) = \mathbf{y}(T+\theta) = \mathbf{a}(\theta)e^{\lambda T} e^{\lambda\theta}, \tag{8}$$

If one substitutes (8) into (6) an infinite dimensional eigenvalue problem can be formulated as

$$((U(T) - \mu\mathcal{I})\mathbf{s})(\theta) = \mathbf{0}, \tag{9}$$

where  $\mathcal{I}$  is an identity operator, the nonzero complex eigenvalue  $\mu = e^{\lambda T}$  is called characteristic multiplier and, according to (8), the complex eigenvector has the form

$$\mathbf{s}(\theta) = \mathbf{a}(\theta)e^{\lambda\theta}. \tag{10}$$

Note that  $\mathbf{s}(\theta)$  is defined over the interval  $\theta \in [-\tau_{\max}, 0]$ . Then, Eq. (9) has a nontrivial solution if

$$\ker\{U(T) - \mu\mathcal{I}\} \neq \{\mathbf{0}\}.$$

The orbital stability of the stationary solution  $\mathbf{q}_p$  of (1) is asymptotically stable if all the infinitely many characteristic multipliers have magnitudes less than one, that is,  $|\mu_m| < 1$ ,  $m = 1, 2, \dots$  (otherwise  $\mathbf{q}_p$  is unstable).  $\mathbf{q}_p$  is marginally stable if one of the multipliers is  $|\mu_c| = 1$ . The original system (1) goes through a secondary Hopf bifurcation if  $\mu_c$  is complex with its conjugate pair. Period doubling (flip) or cyclic fold (saddle-node) bifurcation occurs if  $\mu_c = -1$  or  $\mu_c = 1$ , respectively.

#### 4. Semi-discretization

The SD method is based on the discretization of the infinite dimensional state space and the periodic coefficients according to the Floquet theory [14]. The zeroth-order SD method was introduced for general DDEs (including distributed and time-varying delays) in [8], while the first- and higher-order SD techniques were presented for point delay in [20,17,21]. Here, the first-order method is applied. The point of the method is that the delayed terms  $\mathbf{y}(t-\tau_j)$  are approximated over the discretization interval  $t \in [t_i, t_{i+1}]$  as

$$\tilde{\mathbf{y}}_{j,i}(t-\tau_j) = \frac{t-\tau_j-(i-r_j)\Delta\theta}{\Delta\theta} \mathbf{y}_{i-(r_j-1)} - \frac{t-\tau_j-(i+1-r_j)\Delta\theta}{\Delta\theta} \mathbf{y}_{i-r_j},$$

where,  $\Delta\theta = \Delta t = T/k$  with  $k$  being an integer approximation parameter,  $r_j = \text{int}(\tau_j/\Delta\theta + 1/2)$  and

$$\mathbf{y}_{i-(r_j-1)} := \mathbf{y}_{t_i}(-r_j-1)\Delta\theta, \quad \mathbf{y}_{i-r_j} := \mathbf{y}_{t_i}(-r_j)\Delta\theta$$

with  $t_i = i\Delta t$ . This way, DDE (4) is approximated by an ordinary differential equation (ODE) over the time interval  $t \in [t_i, t_{i+1}]$  as

$$\dot{\mathbf{y}}(t) = \mathbf{L}_i \mathbf{y}(t) + \sum_{j=1}^{N_\tau} \mathbf{R}_j(t) \tilde{\mathbf{y}}_{j,i}(t-\tau_j), \tag{11}$$

where the time-periodic coefficient matrix  $\mathbf{L}(t)$  is approximated by the average

$$\mathbf{L}_i = \frac{1}{\Delta t} \int_{t_i}^{t_{i+1}} \mathbf{L}(t) dt.$$

With the help of the analytical solution of Eq. (11), one can formulate a linear map which projects the solution to the next time step

$$\mathbf{z}_{i+1} = \mathbf{B}_i \mathbf{z}_i, \tag{12}$$

where  $\mathbf{z}_i = \text{col}(\mathbf{y}_i, \mathbf{y}_{i-1}, \dots, \mathbf{y}_{i-r})$  with  $r = \text{int}(\tau_{\max}/\Delta\theta + 1/2)$ . Matrix  $\mathbf{B}_i$  is actually the discrete representation of the solution operator  $U(t)$  over the time interval  $t \in [t_i, t_{i+1}]$ . Multiple application of (12) results in

$$\mathbf{z}_{i+k} = \mathbf{\Phi} \mathbf{z}_i = \mathbf{B}_{i+k-1} \mathbf{B}_{i+k-2} \dots \mathbf{B}_{i+1} \mathbf{B}_i \mathbf{z}_i,$$

where the transition matrix  $\mathbf{\Phi}$  is a finite dimensional discrete approximation of the infinite dimensional monodromy operator  $U(T)$ . The (finitely many) eigenvalues of the transition matrix are close to the multipliers of the monodromy operator depending on the step size  $U(T)$  of the discretization. This explains why the stability diagrams constructed by the SD method reliably approximate the exact stability boundaries. The discrete representation of the eigenvalue problem (9) can now be formulated as

$$(\mathbf{\Phi} - \mu \mathbf{I}) \mathbf{S} = \mathbf{0}, \tag{13}$$

where  $\mathbf{I}$  is a unit matrix and  $\mathbf{S}$  is the discrete approximation of the eigenvector  $\mathbf{s}(\theta)$  defined at (10). If  $|\mu_m| < 1$  for all  $m$ , then the system is predicted to be asymptotically stable.

#### 5. Multiple vibration frequencies

The stability boundaries are the lines in the parameter plane where critical multipliers (i.e.,  $|\mu_c| = 1$ ) occur. In one side of these boundaries (usually below), the operation is stable and the tool vibration tends to the time-periodic stationary orbit  $\mathbf{q}_p$ . In the other side of the boundaries, the system loses its stability and it approaches a higher amplitude stable attractor as a threshold of the unstable motion. These non-smooth orbits are referred as chatter vibration in the machine tool industry. Note that this ‘outside’ attractor, according to its non-smooth sense, can simply be a stable periodic orbit, quasi-periodic orbit or a stable chaotic attractor [22,23]. All of these structures are basically originated from the orbits occurred at the linear stability limit, which means the spectra of these non-smooth orbits (chatter) contain the mark of the just-bifurcated orbits. This explains the practical observation that the measured spectrum is close to the one predicted based on linear theories, only.

If the initial state is in the form  $\mathbf{y}_0(\theta) = \sum_{m=1}^{\infty} b_m \mathbf{s}_m(\theta)$ , then, according to (8) and (10), the solution at each period is given

$$\mathbf{y}_{pT}(\theta) = b_1 \mu_1^p \mathbf{s}_1(\theta) + b_2 \mu_2^p \mathbf{s}_2(\theta) + \dots + b_c \mu_c^p \mathbf{s}_c(\theta) + \bar{b}_c \bar{\mu}_c^p \bar{\mathbf{s}}_c(\theta) + \dots \tag{14}$$

Eq. (14) shows that all of the terms will die out except the critical one(s) if  $p$  is sufficiently large, since all the other characteristic multipliers are in modulus less than one, i.e.,

$$\mathbf{y}_{pT}(\theta) \approx b_c \mu_c^p \mathbf{s}_c(\theta) + \bar{b}_c \bar{\mu}_c^p \bar{\mathbf{s}}_c(\theta).$$

Consequently, the critical characteristic exponents in (7) corresponding to the critical characteristic multipliers can be derived using complex logarithm, that is,

$$\ln|\mu_c| + i(\arg\mu_c + 2q\pi) = \lambda_{c,q} T,$$

where  $\lambda_{c,q} = \alpha_c + i\omega_{c,q}$  ( $q$  can be any integer number) and the multiple frequencies can be expressed as

$$\omega_{c,q} = |\omega_{c,b} + \Omega q|, \quad \text{where } \Omega = 2\pi/T. \tag{15}$$

Here  $\omega_{c,b} := \omega_{c,0} = (\arg\mu_c)/T$  is the base frequency that can be calculated directly from the critical multiplier and it indicates the lowest possible vibration frequency, which satisfies the linear map (6) formulated by the Floquet theorem, i.e.,  $T\omega_{c,b} \in [-\pi, \pi]$ . Eq. (15) implies that infinitely many vibration frequencies arise in the spectrum. These frequencies are separated by the principle frequency  $\Omega$  as it was shown in [1] and also coincides with [6]. Note that along the stability boundaries, the critical asymptotic part  $\alpha_c$  is zero, but in practise during the preparation of a stability chart the calculated points are never lying exactly on the border. Thus, for the further investigations  $\alpha_c = (\ln|\mu_c|)/T$  should also be considered. Using the SD method at a point in the vicinity of the stability border, the approximated spectrum of the monodromy operator can be calculated and the critical multiplier  $\mu_c$  and the

discretized version of the corresponding eigenvector  $\mathbf{S}_c$  can be determined numerically (see (13)). The definition of the eigenvectors at (10) gives the possibility to construct the time-periodic term of the critical eigenvector and to write it in Fourier series form

$$\mathbf{a}_c(\theta) = \mathbf{s}_c(\theta) e^{-\lambda_{c,b}\theta} = \sum_{q=-\infty}^{\infty} \mathbf{a}_{c,q} e^{iq\Omega\theta}, \quad (16)$$

where  $\lambda_{c,b} = \alpha_c + i\omega_{c,b}$ . Consider that, any  $\lambda_{c,q}$  can be substituted instead of  $\lambda_{c,b}$  in (16), since  $e^{\lambda_{c,q}T} = \mu_c$ , but that might cause numerical and indexing difficulties in the later analysis. In order to obtain the dominant vibration level, the velocity of the vibration should be considered. According to (5) the Fourier coefficient vectors can be decomposed to parts corresponding to the modal displacement and velocities as

$$\mathbf{a}_{c,q} = \text{col}(\mathbb{a}_{c,q}, \mathbb{v}_{c,q}). \quad (17)$$

In this way, the dominant vibration frequency is associated with the maximum (highest infinite norm) of the calculated Fourier coefficients of the vibration velocity. An implicit formula for the dominant frequency ratio  $q_d$  can be given as

$$v_{c,\max} = v_{c,q_d} = \max_{q=-\infty}^{\infty} \|\mathbb{v}_{c,q}\|_{\infty}. \quad (18)$$

Note that any eigenvectors  $\mathbf{s}(\theta)$  and any of their periodic terms  $\mathbf{a}(\theta)$  are defined in the interval  $\theta \in [-\tau_{\max}, 0]$ . This may cause representation problem of  $\mathbf{a}(\theta)$ , since the condition  $\tau_{\max} = T$  does not hold in all cases, e.g. for uneven pitch cutters [16]. In this case, mathematically, only the truncated versions of the eigenvectors are available, which means their 'periodic' terms cannot be restored in the entire period. In order to overcome this issue, the interpretation of the state  $\mathbf{y}_t(\theta)$  should be given over an extended interval  $\theta \in [-T, 0]$  corresponding to the principal period  $T$  of the milling process.

Using the SD method, only the discrete representation of the critical eigenvectors can be determined in the following form

$$\mathbf{S}_c = \text{col}(\mathbf{S}_{c,i}, \mathbf{S}_{c,i-1}, \dots, \mathbf{S}_{c,i-r}). \quad (19)$$

The elements of the discretized critical eigenvector in (19) contain parts associated with modal displacement and velocity as  $\mathbf{S}_{c,i} = \text{col}(\mathbb{S}_{c,i}, \mathbb{V}_{c,i})$ , similarly in (17). The discrete counterpart of the periodic terms can be defined based on (16) in the form

$$\mathbf{A}_c = \begin{bmatrix} \mathbf{A}_{c,i} \\ \mathbf{A}_{c,i-1} \\ \vdots \\ \mathbf{A}_{c,i-r} \end{bmatrix} = \begin{bmatrix} \mathbf{S}_{c,i} e^{-\lambda_{c,b} \cdot 0} \\ \mathbf{S}_{c,i-1} e^{\lambda_{c,b} \Delta\theta} \\ \vdots \\ \mathbf{S}_{c,i-r} e^{\lambda_{c,b} r \Delta\theta} \end{bmatrix}, \quad (20)$$

where again  $\mathbf{A}_{c,i} = \text{col}(\mathbb{A}_{c,i}, \mathbb{V}_{c,i})$  as in (17). Note that, the parts corresponding to the modal displacement and velocities are vectors defined based on the modal directions  $\mathbf{q}$  in the form

$$\mathbb{A}_{c,k} = \begin{bmatrix} A_{c,k,q_1} \\ A_{c,k,q_2} \\ \vdots \\ A_{c,k,q_n} \end{bmatrix} \quad \text{and} \quad \mathbb{V}_{c,k} = \begin{bmatrix} V_{c,k,q_1} \\ V_{c,k,q_2} \\ \vdots \\ V_{c,k,q_n} \end{bmatrix},$$

where  $k = i, i-1, \dots, i-r$ . The vector  $\mathbf{A}_c$  is periodic and has the form on which low resolution Discrete Fourier Transform (DFT) or Fast Fourier Transform (FFT) can be applied in each modal direction. Depending on the resolution of the discretization described at (12), finite many approximations of the Fourier coefficients  $\mathbf{a}_{c,q}$  can be determined in this manner.

During the construction of the transition matrix  $\Phi$  some irrelevant directions can be omitted in order to speed up the sometimes costly calculation [24,17]. Basically, in milling the ignored directions are the past modal velocities  $\dot{\mathbf{u}}(t+\theta)$ , where

$\theta \in [-\tau_{\max}, 0)$ , since these do not influence the dynamics. Therefore,  $\mathbb{v}_{c,q}$  from (17) cannot be determined directly by DFT or FFT from  $\mathbf{A}_c$ , instead one can calculate the approximate Fourier coefficients of the vibration levels as  $\mathbb{v}_{c,q} = i\omega_{c,q} \mathbb{a}_{c,q}$ .

The dominant frequency ratio  $q_d$  can be determined from the resultant approximate Fourier coefficients  $\mathbb{v}_{c,q}$  applying (18). Consequently, the dominant vibration frequency is given by

$$\omega_{c,d} := \omega_{c,q_d} = |\omega_{c,b} + \Omega q_d|, \quad (21)$$

according to (15).

The major advantage of the above elucidated method is that it does not have a noticeable effect on the speed of the SD technique. Since the size of the window equals to the principle period  $T$ , the DFT or the FFT provides a spectrum with the resolution of the principle frequency  $\Omega = 2\pi/T$  [25]. Consequently, the discrete peaks actually coincide with original peaks  $\mathbf{a}_{c,q}$ , which are distributed also by the principle frequency  $\Omega$  due to its definition in (16). In this way the dominant frequencies can be calculated efficiently along the stability limits and an additional frequency plot can be provided above the stability diagram. One can plot the harmonics of the dominant vibration frequencies and represent their weights based on their amplitudes. This frequency plot may help to identify the source of certain vibrations occurring during machining.

## 6. Case study

In this section the calculation is shown through an example of half-immersion down-milling operation with a three fluted cutter taken from [15]. Two modes in orthogonal directions of the tool-holder-spindle structure are considered with the modal parameters shown in Table 1. As it is shown by the modeshape vectors  $\mathbf{P}_1$  and  $\mathbf{P}_2$  the modes coincide with the (x) and (y) directions.

The calculations were done using first order SD method with  $N_{SD} = 90$  elements to discretize the state  $\mathbf{y}_t(\theta)$ . The stability chart shown in Fig. 2b was created by fractal method based on triangle elements. The spectra of the discrete periodical 'terms'  $\mathbf{A}_c$  of the critical eigenvectors were calculated at the closest points of the stability limits. In the frequency plot in Fig. 2a the dominant vibration frequencies are indicated by black colour along the stability boundaries. The strengths of the other harmonics were indicated by grey-scale except the peaks that are less than 20% compared to the strength of the dominant frequency. Certain resonant frequencies  $\Omega_l = \omega_{n,l}/N$  of the modes are pointed out in Fig. 2 referring to the resonant spindle speeds, the flip regions and the mode interaction zones [26]. In Fig. 2a one can follow that the dominant vibration frequencies are in most of the cases close to the natural frequencies. Point D corresponds to period doubling (flip) bifurcation that can be recognized in Fig. 2a as the frequencies are lying on the lines that are odd multiples of a straight line with slope 1/2 [27]. Points B and D represent simple cases, when only the dominant frequency is strong. For points A and C some other harmonics also show up besides the dominant one. The relevant multipliers with the unit circle are depicted in Fig. 2b and the type of the stability loss can be associated in this way at points (A, B, C, D).

**Table 1**

The modal parameters of the modes considered in the calculation of the case study corresponding with Fig. 1.

$l$	$\omega_{n,l}$ (Hz)	$\xi_l$ (%)	$k_l$ (N/ $\mu\text{m}$ )	$\mathbf{P}_l$
1	510	4	96.2	$[1 \ 0]^T$
2	802	5	47.5	$[0 \ 1]^T$

Fig. 3a,b show the discretized critical eigenvectors  $\mathbf{S}_c$  (19) and their periodic ‘terms’  $\mathbf{A}_c$  (20). More strictly, to ease the depiction, only the real part of the displacement parts of  $\mathbf{S}_c$  and  $\mathbf{A}_c$  are showed, namely the  $\text{Re } \mathbf{S}_{c,k}$ ’s and  $\text{Re } \mathbf{A}_{c,k}$ ’s ( $k=i,i-1,\dots,i-r$ ). In panels (a) and (b) the values at  $\theta=0$  correspond to  $\mathbf{S}_{c,i}$  and  $\mathbf{A}_{c,i}$ , while the values at  $\theta=-\tau_{\max}$  correspond to  $\mathbf{S}_{c,i-r}$  and  $\mathbf{A}_{c,i-r}$ , respectively. If  $\tau_{\max}=T$  the discrete representation  $\mathbf{A}_c$  of the periodic term  $\mathbf{a}_c(\theta)$  is complete, that is,  $\mathbf{A}_{c,i}=\mathbf{A}_{c,i-r}$  in Fig. 3. The black and the grey dots refer to the two modal directions  $q_1$  and  $q_2$  of the model. The spectra  $v_{c,q}$  (17) determined by the SD method and the FFTs of the modal velocity  $\dot{\mathbf{u}}(t)$  (5) calculated by

time domain simulations (standard DDE23 routine in MATLAB) of the variational system (4) are depicted in Fig. 3c. One can immediately recognize (Fig. 3a) that the eigenvectors  $\mathbf{S}_c$  are not time-periodic as it was expected at (10). They oscillate around zero, since those eigenvectors are derived from the variational system where, in fact, the amplitude of the theoretical stationary solution is zero. The periodic ‘terms’  $\mathbf{A}_c$ , however, may have non-oscillating component, too (see e.g. point D in Fig. 3b). In this case the dominant vibration frequency is actually the calculated base frequency  $\omega_{c,b}$ , that is,  $q_d=0$  (cf. (15) and (18)). In all of the other cases for points (A, B and C) the periodic terms seem to oscillate around zero, since they have different dominant vibration frequency as the base one, thus,  $q_d$  is nonzero (see the triangles denoting the base frequencies in Fig. 3c).

### 7. Experimental verification

The presented method to predict the dominant vibration frequencies was verified experimentally. In this section, we give an overview of the measurement and the results of the tests performed using conventional milling operation.

#### 7.1. Measurement environment

A measurement setup shown in Fig. 4 was created to have a clear and flexible mode perpendicular to the feed direction ( $x$ ). Four modes (one in the ( $x$ ) and three in the ( $y$ ) directions) and the corresponding modal parameters are given in Table 2. A continuous variation of the axial depth of cut  $a_p$  was achieved by using a

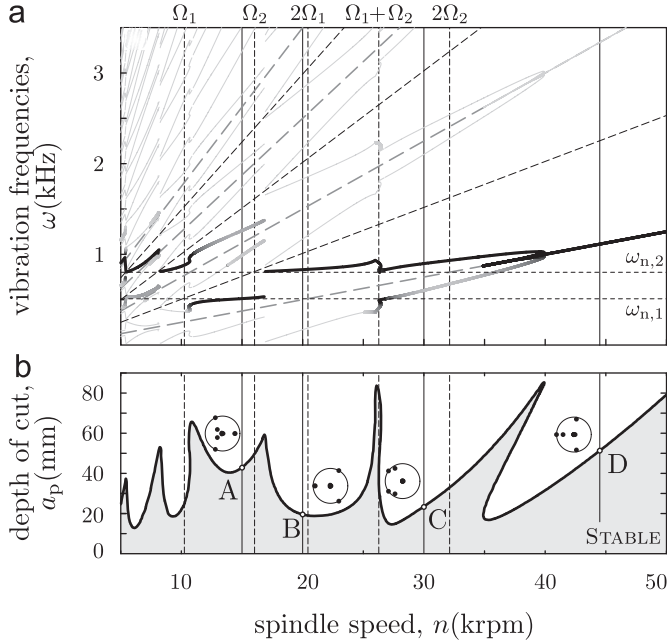


Fig. 2. Panel (a) shows the dominant vibration frequencies (black) along the stability border. The strengths of the harmonics are indicated by grey-scale.  $\omega_{n,l}$  ( $l=1,2$ ) are the natural frequencies of the modes considered in the calculation. Panel (b) shows the stability chart and the unit circles with the multipliers in the complex plain for points (A, B, C, D). (Here,  $K_t=900 \text{ N/mm}^2$  and  $K_r=270 \text{ N/mm}^2$ ).

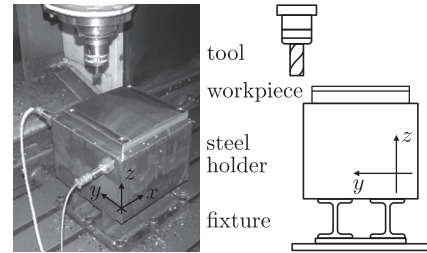


Fig. 4. Shows the measurement arrangement used for chatter tests.

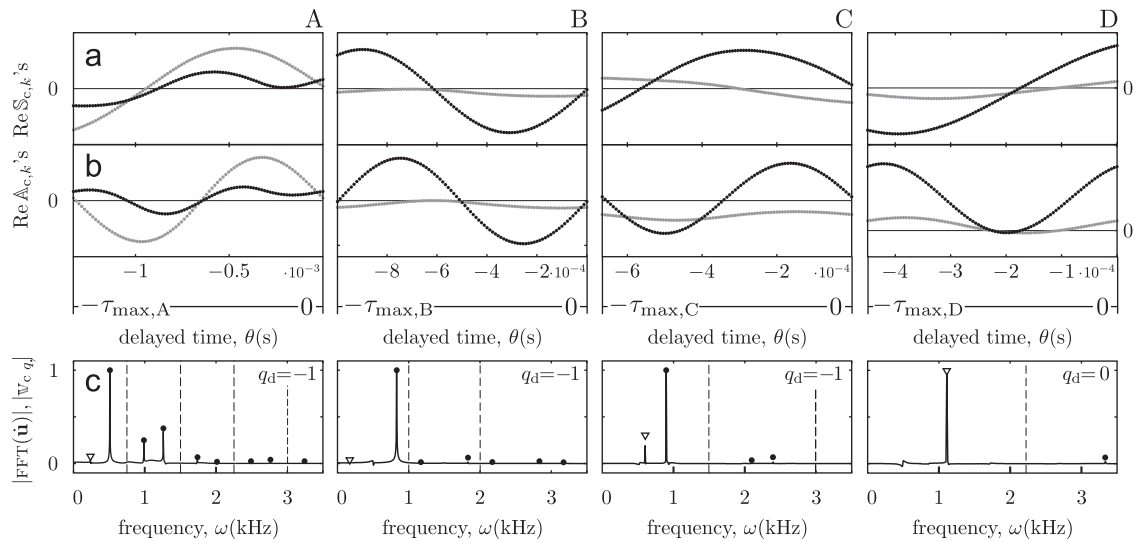


Fig. 3. Panels (a) show the critical eigenvectors of the transition matrix. In panels (b) the periodic terms of the critical eigenvectors are depicted. Panels (c) present the FFT’s of the periodic terms (denoted by black dots) and the FFT’s of time domain simulations of the variational system (4) (denoted by continuous line). The triangles mark the base vibration frequency  $\omega_{c,b}$ . Dashed lines denote the tooth passing frequencies.

ramp-like (or roof-like) mirror slope on steel (C45) workpiece with 5 mm highest axial depth of cut in the middle (see Fig. 5d). This strategy can lead to a more accurate and also quicker

determination of the practical limit of the stability than the often used ‘step-cutting’ strategy. However, the identification of the accurate depth of cut is not clear. Here, the average depths of cut of the individual teeth were considered, which yields to a shift ( $D/\pi$ ) of the effective position compared to the centre of the tool (thin vertical line in Fig. 5d). The tool was a four fluted  $N=4$  inserted cutter with helix angle  $\eta \approx 20^\circ$  and diameter  $D=32$  mm. Because of the limited width of the workpiece near full-immersion milling was performed successively side by side with 31 mm radial immersion. This causes  $20.36^\circ$  deviation in the entry angle  $\varphi_{en}$  (see Fig. 1) compared to the perfect arrangement. Preliminary tests were performed to identify the cutting coefficients of the linear cutting force model [28]. The tangential and the radial

**Table 2**  
The modal parameters of the measurement setup.

$l$	$\omega_{n,l}$ (Hz)	$\xi_l$ (%)	$k_l$ (N/ $\mu\text{m}$ )	$\mathbf{P}_l$
1	94	0.66	58.38	$[0 \ 1]^T$
2	230.6	1	161	$[1 \ 0]^T$
3	336.3	0.3	773.4	$[0 \ 1]^T$
4	375.6	1	632	$[0 \ 1]^T$

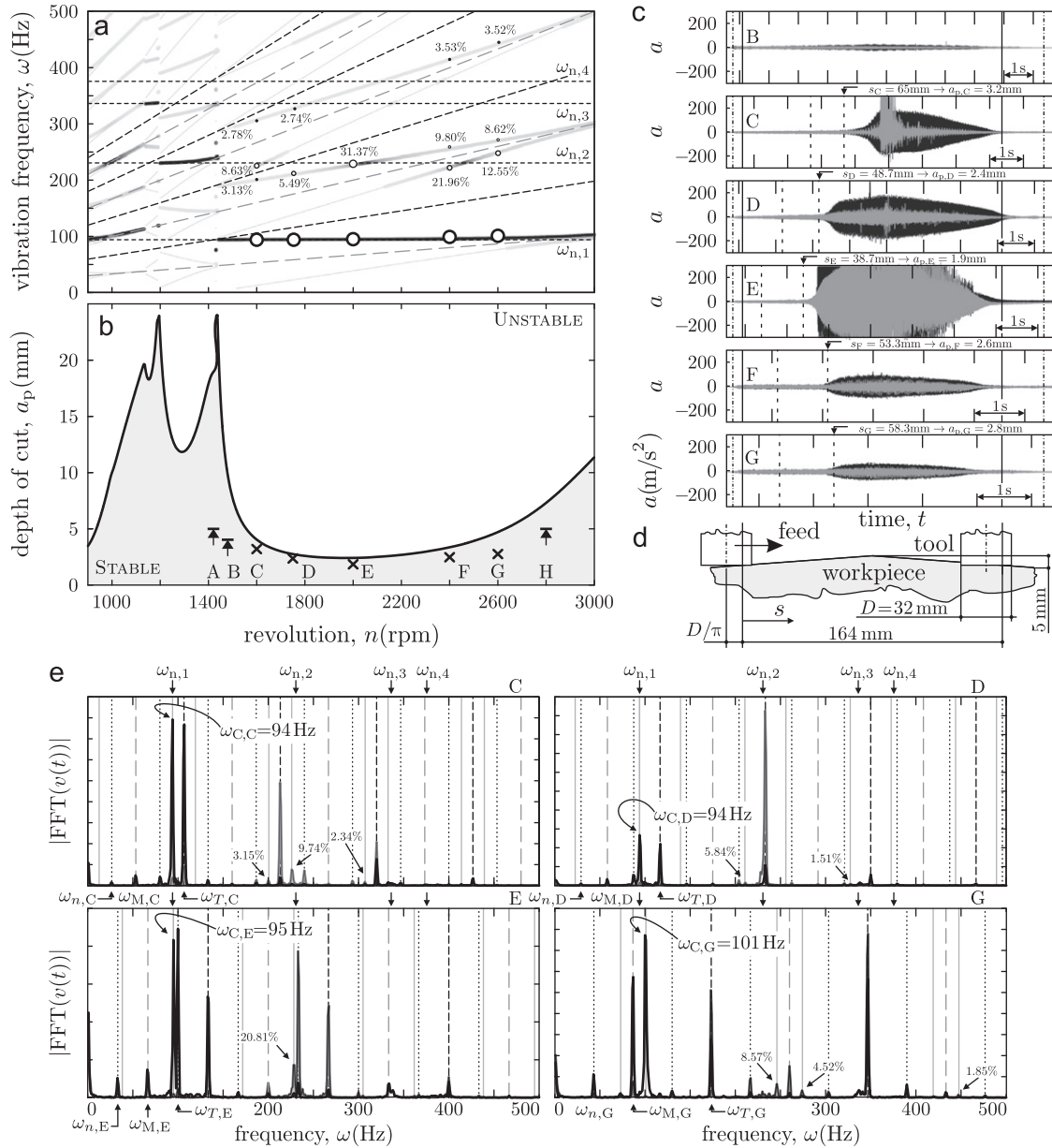


**Fig. 5.** Panel (b) and (a) show the stability chart and the frequency diagram of the full immersion milling process. In panel (a) the black and thick lines denote the dominant self-excited vibration frequencies along the stability limits, while the weaker frequencies are showed by thick grey-scale. The measured frequency peaks are indicated by circles of sizes proportional to their strengths (cf. (e)). In panel (b) the crosses mark the limit depths of cut that were reached by stable machining using test arrangement depicted in (d). Six samples of acceleration signals are plotted in (c). The spectra in panels (e) correspond to the critical windows of STFT denoted by dashed lines in panels (c). In (c) and (e) the black and grey colours are associated with the (y) and the (x) directions, respectively (cf. Fig. 4). In panel (a) and (e) the dashed black lines, the grey dashed lines and the black dotted lines indicate the tooth passing frequencies  $\omega_T$ , the flip-lines  $\omega_M$  and the spindle frequencies  $\omega_n$  and their harmonics, too. The measured dominant chatter peaks are marked by  $\omega_C$  with their actual values given in (e).

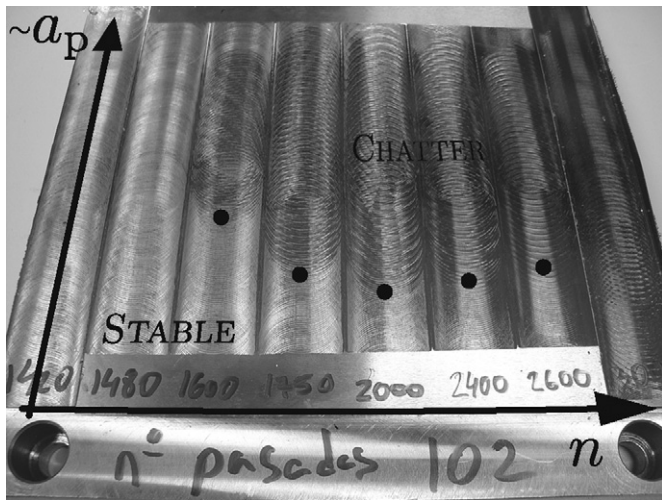


Fig. 6. Shows the workpiece after all test were performed. The marks left by the chattering tool can be realized easily.

cutting coefficients were  $K_t=1459 \text{ N/mm}^2$  and  $K_r=259 \text{ N/mm}^2$ , respectively.

During the measurements accelerations were collected by a data acquisition system in the feed direction ( $x$ ) and the direction perpendicular to the feed ( $y$ ). Eight different speeds were selected and six of those are shown in Fig. 5c, where black and grey colours correspond to the ( $y$ ) and ( $x$ ) directions, respectively. The selected speeds were:  $n_{A,B,C,D,E,F,G,H}=1420, 1480, 1600, 1750, 2000, 2400, 2600, 3000 \text{ rpm}$ . The maximum axial depths of cut were kept to be 4 mm for safety reasons except the measurements A and H that were both stable all along the shots (cf. Fig. 6). One can directly realize by means of the measurement-sketch in Fig. 5d that the cutting process jumped to chatter at higher axial depths of cut than it restored to stationary cutting. This can be explained by the so-called unsafe zones, which are the effect of the nonlinearities occurring in the cutting force characteristics [29–31].

## 7.2. Evaluation of the results

The limit depths of cut were calculated indirectly from the measured motion of the tool  $s$  using the actual time when the tool entered into the slope, the time when it lost its stability and the feed  $f=0.8 \text{ mm/rev}$ . The instant of entrance into the workpiece can be obtained directly from the time domain representation of the signals (Fig. 5c). But, in order to have the instant of stability loss, the strength of the just-developing-frequency of the self-excited vibration (in practise the so-called chatter frequency,  $\omega_c$ ) needs to be compared with the strongest peak of the forced vibration (usually the peak of the tooth passing frequency,  $\omega_T$ ) related to the same direction. For this purpose, short-time Fourier transform (STFT) was applied on the time signals using sliding Hann window of length 1 s with time-step 0.1 s and the spectra were transformed to vibration level  $|\text{FFT}(v(t))|$  in frequency domain. The process was declared to be unstable when the peaks of the self-excitation and the corresponding forced vibration were roughly equal and the position of the moving tool was determined at that time. Using this strategy relatively large error on the tool-position  $s$  results in negligible error on the axial depth of cut due to the gentle slope. In Fig. 5b the measured stability limits are indicated by crosses while the stable shots are by arrows with tips up to the reached maximum depths of cut. Compared with the predicted stability limit (solid line) the trend of the large 'lobe' can be recognized.

The predicted frequencies of the self-excited vibrations and their harmonics are plotted in Fig. 5a by thick grey-scale, so that, the dominant vibration frequencies  $\omega_{c,d}$  (21) are black, while the weaker ones are grey proportional to their strengths. The thin grey lines show the non-operating (with strengths less than 2.5%) multiple harmonics  $\omega_{c,q}$  (15) of the dominant frequencies. The horizontal and the inclined dashed black lines indicate the natural frequencies  $\omega_{n,1..4}$  (Table 2) and the tooth passing frequencies  $\omega_T=Nn/(60 \text{ s/min})$  and their harmonics. The lines  $\omega_M=\omega_T/2$  and their harmonics, on which the frequencies of the double period (flip) self-excited orbits can lay, are marked by inclined grey dashed lines [27].

According to Fig. 5a two things can be realized directly. On the one hand, only the first three modes have effect on the stability since the dominant frequencies lay close to the first three natural frequencies  $\omega_{n,1..3}$ . On the other hand some harmonics of the self-excited frequencies are active (grey-scale), but in the region of the measurements ( $n \in [1400, 3000] \text{ rpm}$ ) only small portions of them are significant. Note that this does not show up in the prediction if one uses exact full-immersion milling model during the calculations. In this case, the inside symmetry due to the full-immersion sense and the approximated circular orbits of the flutes make the periodical force smoother than it is in the reality. Generally, the predicted frequencies agree well with the measured spectrum (chatter frequencies and their harmonics) depicted by circles in Fig. 5a. The size of the circles are proportional to the measured peaks and the values next to the circles show the strength of the predicted peaks (in percentage) compared with the strength of the dominant frequency.

The critical STFT intervals, where the signs of the stability loss were first identified are denoted by dashed lines in Fig. 5c. The FFTs of the signal over the critical intervals are presented in panels (e) for cases C, D, E and G. The continuous and dashed guidelines in panels (e) correspond to those in Fig. 5a, while dotted lines denote the harmonics of the spindle frequency  $\omega_n=n/(60 \text{ s/min})$ . The grey and black lines indicate the spectra in direction of ( $y$ ) and ( $x$ ). In all samples, the peaks that do not coincide with any harmonics of the spindle frequencies are the frequencies of the self-excited vibrations (practically the chatter frequencies  $\omega_c$ ) or their harmonics. One can realize that these samples are taken from the critical intervals since the chatter peaks are about the level of the strongest forced frequency. Note that for case D, the strongest forced frequency is in the feed direction ( $x$ ), while chatter occurs in the perpendicular ( $y$ ) direction. For case E, the third spindle harmonic (arising due to the possible run-out of tool) is the strongest forced peak since it is in resonance with the first natural frequency of the system  $\omega_{n,1}$  (see arrows above the frames of Fig. 5e). It can be seen that the level of the chatter peaks and their harmonics correlate well to the predicted frequencies and their level shown by grey-scale in panel (a). The second mode, which is in the feed direction, resonates with the harmonics of the self-excited vibration. This phenomenon is similar to the so-called mode interaction introduced in [26].

Even though plain milling was performed, face of the milling cutter leaves strong marks on the workpiece during chattering motion due to the bending vibrations of the tool. This results in an indirect visible manifestation of the stability lobes on the workpiece shown in Fig. 6.

Using the strategy of the stability-loss-detection applied here combined with a fast stability prediction can give a tool in real-time stabilization of milling processes. As it can be followed in Fig. 5c the loss of stability was detected much before the onset of the large amplitude chatter vibration (cf. the length of the critical windows in Fig. 5c). For case C, for instance, the detection was around a second before the chatter was fully developed. This may give possibilities to introduce real-time controlling techniques based on stability diagrams.

## 8. Conclusions

We have focussed on the determination of the dominant vibration frequencies of milling processes using the semi-discretization method. The algorithm shown here can predict the strengths of the multiple vibration frequencies with no significant computational cost. The given method is based on the governing time-periodic delay differential equation of general milling processes and hence it can handle complex geometries and dynamics of the tool-spindle-machine system. Besides the stability charts of the process, our method provides a visual and useful representation of the operating frequencies during machining. This might be important even at the stage of machine tool design.

We have determined the dominant frequency among the multiple frequencies of the developing self-excited vibration (chatter) according to rigorous mathematical theories. We showed that the ratio of the dominant frequency and the principal (e.g. tooth passing) frequency is hidden in the eigenvectors of the fundamental operator defined by the Floquet theory. A periodic function can be constructed analytically using the eigenvectors and the characteristic multipliers. Then, low resolution DFT or FFT can be applied on the discretized counterparts of these periodic functions without having significant effect on the computational speed of the semi-discretization. In this way, the weight of the individual chatter frequency harmonics can be determined efficiently.

An artificial, but representative example was shown, in which all the effect of the multiple vibration frequencies of the self-excited vibration can be followed easily on the frequency plot. In this plot, it is easy to recognize simple and more complex cases where e.g. different modes of the system interact with the self-excitation.

As a practical vindication, we have performed milling tests using ramp-like workpiece fixed on a special holder which has a main mode perpendicular to the feed direction. Besides the linear stability limits, the semi-discretization predicted the dominant frequencies, as well. Moreover, it showed the effect that other modes of the system can resonate with the harmonics of the dominant frequency of the self-excited vibration (in practise the chatter frequency).

## Acknowledgements

This work was partially supported by the Janos Bolyai Research Scholarship of the Hungarian Academy of Sciences, the Hungarian National Science Foundation under Grant no. K72911, New Hungary Development Plan (Project ID: TÁMOP-4.2.1/B-09/1/KMR-2010-0002) and the OPENAER project (CENIT program of Technical Industrial Development Center (CDTI) of the Spanish government). And special thanks for Zekai Murat Kilic, Manufacturing Automation Laboratory, UBC.

## References

- [1] T. Insperger, G. Stepan, P. Bayly, B. Mann, Multiple chatter frequencies in milling processes, *Journal of Sound and Vibration* 262 (2) (2003) 333–345.
- [2] J. Tlustý, L. Spacek, Self-excited vibrations on machine tools, *Nakl. CSAV*, 1954 (in Czech).
- [3] S. Tobias, *Machine-Tool Vibration*, Blackie, 1965.

- [4] E. Ezugwu, Key improvements in the machining of difficult-to-cut aerospace superalloys, *International Journal of Machine Tools and Manufacture* 45 (2005) 1353–1367.
- [5] Y. Altintas, E. Budak, Analytical prediction of stability lobes in milling, *CIRP Annals—Manufacturing Technology* 44 (1995) 357–362.
- [6] E. Budak, Y. Altintas, Analytical prediction of chatter stability in milling—part I: general formulation, *Journal of Dynamic Systems, Measurement, and Control* 120 (1) (1998) 22–30.
- [7] S.D. Merdol, Y. Altintas, Multi frequency solution of chatter stability for low immersion milling, *Journal of Manufacturing Science and Engineering* 126 (3) (2004) 459–466.
- [8] T. Insperger, G. Stepan, Semi-discretization method for delayed systems, *International Journal for Numerical Methods in Engineering* 55 (2002) 503–518.
- [9] P. Bayly, J. Halley, B. Mann, M. Davies, Stability of interrupted cutting by temporal finite element analysis, *Journal of Manufacturing Science and Engineering* 125 (2) (2003) 220–225.
- [10] R. Szalai, G. Stepan, S. Hogan, Continuation of bifurcations in periodic delay-differential equations using characteristic matrices, *Chaos* 28 (4) (2006) 1301–1317.
- [11] S.D. Merdol, Y. Altintas, Mechanics and dynamics of serrated cylindrical and tapered end mills, *Journal of Manufacturing Science and Engineering* 126 (2) (2004) 317–326.
- [12] W.B. Ferry, Y. Altintas, Virtual five-axis flank milling of jet engine impellers—part I: mechanics of five-axis flank milling, *Journal of Manufacturing Science and Engineering* 130 (1) (2008) 011005.
- [13] Z. Dombovari, Y. Altintas, G. Stepan, The effect of serration on mechanics and stability of milling cutters, *International Journal of Machine Tools and Manufacture* 50 (1) (2010) 511–520.
- [14] M. Farkas, *Periodic Motions*, Springer-Verlag, Berlin, New York, 1994.
- [15] Y. Altintas, G. Stepan, D. Merdol, Z. Dombovari, Chatter stability of milling in frequency and discrete time domain, *CIRP, Journal of Manufacturing Science and Technology* 1 (1) (2008) 35–44.
- [16] E. Budak, An analytical design method for milling cutters with nonconstant pitch to increase stability, part I: theory, *Journal of Manufacturing Science and Engineering* 125 (1) (2003) 29–35.
- [17] T. Insperger, G. Stepan, J. Turi, On the higher-order semi-discretizations for periodic delayed systems, *Journal of Sound and Vibration* 313 (2008) 334–341.
- [18] J. Hale, *Theory of Functional Differential Equations*, Springer-Verlag, New York, 1977.
- [19] G. Stépán, *Retarded Dynamical Systems*, Longman, London, 1989.
- [20] O. Elbeyli, J. Sun, On the semi-discretization method for feedback control design of linear systems with time delay, *Journal of Sound and Vibration* 273 (2004) 1–2.
- [21] T. Insperger, Full-discretization and semi-discretization for milling stability prediction: some comments, *International Journal of Machine Tools and Manufacture* 50 (7) (2010) 658–662.
- [22] Z. Dombovari, D.A. Barton, R.E. Wilson, G. Stepan, On the global dynamics of chatter in the orthogonal cutting model, *International Journal of Non-Linear Mechanics* 46 (1) (2011) 330–338, doi:10.1016/j.jnonlinmec.2010.09.016.
- [23] P. Wahi, A. Chatterjee, Self-interrupted regenerative metal cutting in turning, *International Journal of Non-Linear Mechanics* 43 (2) (2008) 111–123.
- [24] C. Henninger, P. Eberhard, Improving the computational efficiency and accuracy of the semi-discretization method for periodic delay-differential equations, *European Journal of Mechanics—A/Solids* 27 (6) (2008) 975–985.
- [25] D. Ewins, *Modal Testing: Theory, Practice, and Applications*, Research Studies Press, 2000.
- [26] J. Muñoz, M. Zatarain, Z. Dombovari, Y. Yang, Effect of mode interaction on stability of milling processes, in: *Proceedings of 12th CIRP Conference on MMO*, Donostia-San Sebastian, Gipuzkoa, Spain, 2009.
- [27] J. Muñoz, Desarrollo de un modelo general para la predicción de la estabilidad del proceso de fresado. aplicación al fresado periférico, al planeado convencional y a la caracterización de la estabilidad dinámica de fresadoras universales, Mondragon University, Ph.D. Thesis (in Spanish).
- [28] Y. Altintas, *Manufacturing Automation: Metal Cutting Mechanics Machine Tool Vibrations and CNC Design*, Cambridge University Press, Cambridge, 2000.
- [29] G. Stepan, T. Kalmar Nagy, Nonlinear regenerative machine tool vibrations, in: *Proceedings of ASME Design Engineering Technical Conference*, Sacramento, California, 1997, DETC97/VIB-4021.
- [30] T. Kalmár Nagy, G. Stepan, F. Moon, Subcritical Hopf bifurcation in the delay equation model for machine tool vibrations, *Nonlinear Dynamics* 26 (2) (2001) 121–142.
- [31] Z. Dombóvári, R. Wilson, G. Stépán, Estimates of the bistable region in metal cutting, *Proceedings of the Royal Society A: Mathematical Physical and Engineering Science* 464 (2100) (2008) 3255–3271.